University of Reading

Working fluid pair selection of thermally integrated pumped thermal electricity storage system for waste heat recovery and energy storage

Article

Published Version

Creative Commons: Attribution 4.0 (CC-BY)

Open Access

Wu, D., Ma, B., Zhang, J., Chen, Y., Shen, F., Chen, X., Wen, C. ORCID: https://orcid.org/0000-0002-4445-1589 and Yang, Y. (2024) Working fluid pair selection of thermally integrated pumped thermal electricity storage system for waste heat recovery and energy storage. Applied Energy, 371. 123693. ISSN 1872-9118 doi: 10.1016/j.apenergy.2024.123693 Available at https://centaur.reading.ac.uk/118674/

It is advisable to refer to the publisher's version if you intend to cite from the work. See Guidance on citing.

To link to this article DOI: http://dx.doi.org/10.1016/j.apenergy.2024.123693

Publisher: Elsevier

All outputs in CentAUR are protected by Intellectual Property Rights law, including copyright law. Copyright and IPR is retained by the creators or other copyright holders. Terms and conditions for use of this material are defined in the End User Agreement.

University of Reading

www.reading.ac.uk/centaur

CentAUR

Central Archive at the University of Reading

Reading's research outputs online

Applied Energy 371 (2024) 123693

Contents lists available at ScienceDirect

Applied Energy

journal homepage: www.elsevier.com/locate/apenergy

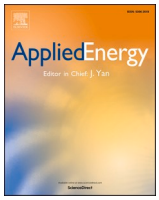

Working fluid pair selection of thermally integrated pumped thermal electricity storage system for waste heat recovery and energy storage

Ding Wu [a], Bo Ma [a,*], Ji Zhang [a], Yanqi Chen [a], Feifan Shen [a], Xun Chen [b], Chuang Wen [c], Yan Yang [d,*]

[a] School of Electrical and Information Engineering, Hunan University, Changsha 410082, China
[b] Research Institute of State Grid Hunan Electric Power Co., Ltd., Changsha 410000, China
[c] School of the Built Environment, University of Reading, Reading RG6 6AH, UK
[d] Faculty of Environment, Science and Economy, University of Exeter, Exeter, EX4 4QF, UK

HIGHLIGHTS

- The double-layer optimization procedure is proposed for working fluid pair screening.
- 3 fluid pair combination strategies are compared under 7 energy storage temperatures.
- The highest round-trip efficiency of 101.29% is obtained by the zeotropic fluid pair.
- Thermo-economic indicators are effectively adjusted by 3 weighting factor groups.
- Working fluid pair recommendations including pure and zeotropic fluids are offered.

ARTICLE INFO

Keywords:
TI-PTES
Energy storage
Waste heat recovery
Zeotropic fluids
Working fluid screening
Pumped thermal electricity storage

ABSTRACT

Global issues such as the energy crisis and carbon emissions impulse the development of waste heat recovery and energy storage technologies. In most practical industrial scenarios, the electricity supply and consumption cannot be perfectly matched and effective utilization of waste heat is in urgent need. In the present study, we develop a mathematical model to evaluate the thermally integrated pumped thermal electricity storage (TI-PTES) system to achieve off-peak electricity storage along with low-grade waste heat recovery. A double-layer optimization for screening working fluid pairs with high round-trip efficiency is carried out from 24 fluids of the heat pump and 21 fluids of the Organic Rankine cycle (ORC). In the first-layer multi-objective optimization, 3 types of working fluid pair combination strategies are compared and the great improvement of round-trip efficiency by using zeotropic fluids is proved. Among 7 energy storage temperatures covering from 393.15 K to 423.15 K with an increment interval of 5 K, the highest round-trip efficiency of 101.29% is achieved by adopting the zeotropic fluid pair [90Diethyl ether_10Pentane - 80Butane_20Pentane] at 398.15 K. Furthermore, in the second-layer single-objective optimization, the thermo-economic performance indicators of TI-PTES is evaluated and compared under different designing weighting factor groups, which effectively contributes to the screening of working fluids according to designer's trade-off. Finally, through varying energy storage temperatures and designing weighting factors, optimal working fluid pair recommendations including pure fluids and zeotropic ones were proposed to the fluid selection of TI-PTES.

1. Introduction

In response to global climate change and the energy crisis, improving energy utilization efficiency, expanding renewable energy resources and devoting to achieving carbon neutrality by 2050 have become a widespread global consensus [1]. Particularly it is crucial to enhance energy utilization efficiency on the customer side of the grid and mitigate substantial carbon emissions from traditional fossil-fuel power plants on the producer side of the grid [2]. In various industry scenarios with high electricity consumption, untapped low-grade waste heat resources are popularly distributed and the investigation of suitable

* Corresponding authors.
E-mail addresses: boma@hnu.edu.cn (B. Ma), y.yang7@exeter.ac.uk (Y. Yang).

https://doi.org/10.1016/j.apenergy.2024.123693
Received 15 January 2024; Received in revised form 18 May 2024; Accepted 9 June 2024
Available online 15 June 2024
0306-2619/© 2024 The Authors. Published by Elsevier Ltd. This is an open access article under the CC BY license (http://creativecommons.org/licenses/by/4.0/).

Nomenclature

Abbreviations

HP	Heat pump cycle
ORC	Organic Rankine cycle
PHES	Pumped hydro energy storage
CAES	Compressed air energy storage
LB	Lithium battery
FB	Flow battery
PTES	Pumped thermal energy storage
SPFS	Single pure fluid strategy
DPFS	Different pure fluids strategy
DFS	Different fluids strategy

Variables

p	Pressure (bar)
c_h	cost of heat energy (€/MWh)
T	Temperature (°C)
Q	Heat load (MW)
m	Mass flow (kg/s)
COP	Coefficient of performance (−)
h	Enthalpy (kJ/kg)
PBT	Payback time (years)
EPC	Electricity production cost (€/MWh)
w	Weighting factor (−)
CF	Cash flow (€)
TCI	Total capital investment (€)
PEC	Purchased equipment cost (€)
CRF	Capital recovery factor (−)
t	Time (hours)
i	Interest rate (%)
f	Cost factor (%)
s	Entropy (kJ/(mol·°C))
η	Efficiency (−)
W	Power (kW)
p_{crit}	Critical Pressure (bar)

Superscript and subscript

in	Inlet
cond	Condenser
ave	Average
e	Exergy efficiency
Lor	Lorenz efficiency
sup	Super heat
evap	Evaporator
crit	Critical
Δ	Difference
pp	Pinch point
sto	Storage
out	Outlet
comp	Compressor
amb	Ambient
wh	Waste heat source
is	Isentropic
rt	Round-trip
net	Net output
cool	Cooling water
cs	Heat sink
eff	Effective
mo	Maintenance and operation
p	Purchasing cost
BM	Basic material
total	Total system
gen	Generated
el	Electricity
op	Operation

energy recovery technology is of great necessity [3]. On the other hand, due to the interest difference between the peak and valley electricity prices of the power grid [4], the efficient power storage system combined with waste heat recovery can reduce the overall carbon emission and expense for large-scale electricity energy utilization factories, that is, to store the valley electricity and waste heat with lower prices and release them during the peak electricity consumption and high carbon emission periods. Besides various electricity storage technologies including compressed air energy storage (CAES), pumped hydro energy storage (PHES), and the chemical battery storage like the flow battery (FB) and lithium battery (LB) [5], there is a growing focus on a novel electricity storage technology known as pumped thermal electricity storage (PTES) in recent years [6]. Providing a geographically unlimited, low-cost and long-lifespan energy storage solution, thermally integrated PTES, named as TI-PTES, can not only utilize the industry waste heat efficiently but also deal with the high expense due to the fluctuation of electricity prices in the power grid, achieving a win-win situation of energy efficiency improvement and cost reduction [7,8].

In order to recycle and utilize the low-grade waste heat in the electricity storage system, the concept of TI-PTES was first proposed by Steinmann in 2014 [9], which typically comprises a heat pump (HP), a heat storage system, and an organic Rankine cycle (ORC) [10]. Through low-grade heat integration and utilization, this approach allows for a reduction in the temperature lift of the HP or an increase in the temperature difference between the heat source and heat sink of the ORC, thereby enhancing the round-trip efficiency (η_{rt}) [11]. Facilitated by the availability of all components of the HP or ORC in the market or given that all components can also be specially designed with greater feasibility, the commercial application maturity of TI-PTES is relatively high [12]. Generally, the research on TI-PTES toward high round-trip efficiency can be classified into three main directions or aspects [10], including system configuration optimization [13,14], working fluids selection [15] and system parameter analysis [16]. As an important aspect of design research, the working fluids selection of TI-PTES is of great necessity and has attracted many scholars' research interests in the past 5 years.

In typical PTES systems, the majority of studies have utilized the same pure working fluid in the HP and ORC, such as R245fa [17], R1233zd(E) [5], Butene [18], etc. Hence, as a branch of PTES, most working fluid selection research of TI-PTES similarly supposed that the HP and ORC had adopted the same working fluid. Frate et al. [15] studied extensively on the working fluid selection from 17 candidates and found that the highest η_{rt} of 130% was obtained by R1233zd(E) among the most 4 environmentally friendly fluids. Eppinger et al. [19] preliminarily selected 4 fluids from 33 fluids for a Rankine PTES. On this basis, Eppinger et al. [20] further made a careful performance comparison among Cyclopentane, R365mfc, Novec 649 and R1233zd(E) for screening the working fluid of a reversible TI-PTES system and R1233zd (E) was considered as the most suitable fluid candidate. A similar conclusion about R1233zd(E) was illustrated in the work of Steger et al. [21] and the study of Ma et al. [22]. In a simplified model for quick analysis [11], Dumont et al. investigated 16 working fluids and only 5 fluids showed a decent efficiency including R1233zd(e), R1234yf, R11, R236ea and R245fa. Under a specific working condition, R245ca was considered to be the most favorable fluid candidate among the 9 primarily selected fluids in Ref. [23]. At the molecular level, Qiao et al. [24] conducted a screening work for the TI-PTES system among 70 working fluids and the highest round-trip efficiency of 57.5% was

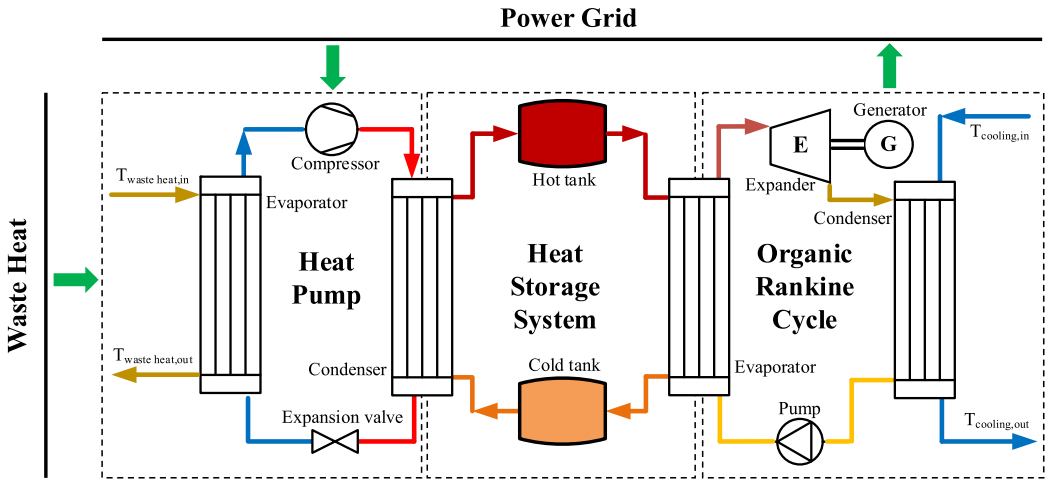

Fig. 1. Description of the TI-PTES system.

obtained by utilizing R272fa. To facilitate the sharing of equipment between the HP and ORC, the same working fluid was applied in Ref. [25] and four fluid candidates were ranked and screened according to the round-trip efficiency (R1233zd(E) > R245fa > Butene > R236ea). Another study conducted by Zhang et al. [26] focused on a comparison among R245fa, R1336mzz(Z), R1233zd(E), and R1234ze(Z) while screening the suitable working fluids for 3 different TI-PTES system configurations. In addition, for the TI-PTES system different pure working fluids have been utilized and examined in the HP and ORC units. To the best knowledge of the authors, only several related articles have been retrieved. Frate et al. [27] investigated exhaustively all the possible working fluid pairs from a representative subset of 8 fluids and suggested different working fluid pairs concerning various monitored performance parameters. Following similar screening principles, Fan et al. [28] selected economic, exergy-economic performance criteria and exergy efficiency as optimization target parameters for seeking the best working fluids pair under different energy storage temperatures. However, only 2 fluids R245fa and R1336mzz(Z) were considered. Recently, a multi-objective optimization from 4 different working fluid combinations was carried out by Wang et al. [29] and the working fluid pair R365mfc/R365mfc achieved the highest round-trip efficiency of 110.15%.

In the interesting work of Hassan et al. [30], both working fluid selection strategies above were applied and they concluded that in a specific energy storage case adopting a single pure working fluid was the best choice while in another case considering the impact on the environment, employing different working fluids was a better strategy. Hence, the working fluid selection strategy should cover all the possibilities of working fluids pair. Another noteworthy research point about working fluid in TI-PTES is the utilization of zeotropic fluids which has been studied extensively in HP or ORC [31–33]. To weaken the mismatch phenomenon of thermal streams in the heat exchangers, the zeotropic mixture of ammonia and water was utilized as the working fluid in a PTES system in Bernehed's work [34]. Lu et al. [35] compared the round-trip efficiency between conventional TI-PTES and TI-PTES using R1233zd(*E*)-Cyclopentane mixed zeotropic fluid and found that round-trip efficiency is improved by 22.40% compared with pure working fluid. Until now, no other PTES system has been reported using a zeotropic mixture as its working fluid.

Despite all these abovementioned studies on the selection of TI-PTES system working fluid pairs, there is a lack of the comprehensive investigation on screening working fluid pairs consisting of different pure fluids or zeotropic fluids. Most of the existing research focuses on working fluid pair screening in the case of employing a single pure working fluid in the TI-PTES system. Several articles primarily analyzed the working fluid pairs consisting of different fluids. While comprehensive investigations to assess the feasibility of employing different fluids have not been conducted in detail. Even though zeotropic working fluids have been proven beneficial to round-trip efficiency improvement in recent two papers, no more research has been published lately. In fact, to achieve a high round-trip efficiency of TI-PTES, a good selection of working fluid pairs is the first step, which, however, has not been studied extensively yet. Investigating working fluid pairs, including combinations of diverse fluids and zeotropic fluids, across varying energy storage temperatures holds significant value in comprehending the potential of these pairs to enhance the performance of TI-PTES, which is the research gap that merits exploration in this study. Hence, the principal contributions of this study can be summarized as following: (1) expansion of the working fluid selection range for the TI-PTES system; (2) investigation into the performance enhancement potential by utilizing different working fluid pairs and types; (3) recommendation for selecting working fluid pairs at various heat storage temperatures, showcasing the system's applicative potential. The arrangement of the research content is delineated as follows: in Section 2, the thermo-economic model is established and validated, with a brief introduction to the dual-layer working fluid screening method. The impact of working fluid pair selection strategies (involving both pure and zeotropic fluids) and energy storage temperatures on the round-trip efficiency is examined in Section 3.1. The results from the second layer of screening are analyzed in Section 3.2, where the effects of user-defined design weighting factors on these results are discussed. Optimal working fluid recommendations under various storage temperatures and design weighting factors are summarized in Section 3.3.

2. Methods

The TI-PTES system studied in this paper is shown in Fig. 1, which consists of the heat pump (HP), heat storage system, and Organic Rankine cycle (ORC). Working as the charging cycle, the HP system receives the low-cost electric power from the off-peak grid and waste heat from the industry manufacturing processes. And the grade-lifted thermal energy is transmitted to the heat storage system. In this way, the off-peak electricity is stored in the form of heat exergy. Working as the discharging cycle, the ORC system enables the energy conversion from stored thermal energy to generated electricity energy in the on-peak electricity consumption period. In this paper, widely adopted sensible heat storage is selected and the high-pressure water at 5 bar is used as the heat storage fluid suggested by previous work [32].

All the heat exchangers are assumed to be plate types for the mature technology and excellent heat transfer performance. The heat transfer

Table 1
Assumed parameters of the TI-PTES system.

Parameter	Symbol	Unit	Value
Heat load of waste heat source	Q_{wh}	MW	3
Inlet temperature of waste heat source	$T_{wh,in}$	K	373.15
Outlet temperature of waste heat source	$T_{wh,out}$	K	348.15
Compressor or Turbine efficiency	η_{comp}/η_{tur}	–	0.75
Pump efficiency	η_{pump}	–	0.85
Motor or Generator efficiency	η_{motor}/η_{gen}	–	0.97
Heat storage efficiency	η_{sto}	–	1
Pinch point temperature difference	ΔT_{pp}	K	3
Superheat degree	ΔT_{sup}	K	5
Cooling water inlet temperature	$T_{cool,inlet}$	K	298.15
Ambient temperature	T_{amb}	K	293.15

Table 2
List of fluids candidates for screening.

Cycle	Working fluids for screening	References
HP	R50, R170, R134a, R1150, R1270, R290, Dimethyl ether (DME), Hexane, Heptane, R600, R600a, R601, R601a, R717, R718, R744, Diethyl ether (DEE), R1224yd(Z), R1233zd(E), R1234ze(E), R1234ze(Z), R1234yf, R1243zf, R1336mzz(Z)	[41–45]
ORC	R161, R290, R1270, R152a, R134a, R123, R227ea, R245fa, R600, R600a, R601, R601a, R1123, R1216, R1224yd(Z), R1233zd(E), R1234ze(E), R1234ze(Z), R1234yf, R1243zf, R1336mzz(Z)	[46–48]

coefficients of plate heat exchangers are given in Ref. [36]. The assumed system parameters are listed as Table 1. In this study, the heat load of the waste heat source (Q_{wh}) is set at 3 MW, aligning with existing theoretical studies where Carnot batteries typically operate in the megawatt range for economic viability and potential market commercialization [25,26]. The inlet ($T_{wh,in}$) and outlet ($T_{wh,out}$) temperatures of the waste heat source are assumed to be 373.15 K and 348.15 K, respectively, based on extensive research on industrial waste heat temperature ranges (353.15 K to 393.15 K) [30,37–40]. These values reflect typical scenarios and a practical temperature drop of 25 K after heat utilization. Additionally, the thermal storage efficiency (η_{sto}) is assumed to be 1 for simplification, as the heat pump, thermal storage, and ORC processes are considered independent, with the selection of working fluids focusing on the charging and discharging cycles under given thermal conditions. This assumption facilitates an ideal proportional scaling of the round-trip efficiency without affecting comparative results between different working fluids. As the working fluid pairs significantly influence the TI-PTES system's round-trip efficiency, in this study, extensive and in-depth research on the screening of work fluid pairs is conducted covering 24 fluids [41–45] for HP and 21 fluids [46–48] for ORC in total shown in Table 2.

2.1. Thermo-economic model

For the investigated TI-PTES system, waste heat and low-cost electricity are energy inputs, and the generated electricity is the energy output transmitted back to the grid. As the core indicator of the energy storage system, the round-trip efficiency (η_{rt}) could be calculated by:

$$\eta_{rt} = \frac{W_{gen}}{W_{comp}} = \frac{Q_{sto}}{W_{comp}} \times \eta_{sto} \times \frac{W_{gen}}{\eta_{sto} Q_{sto}} = COP \times \eta_{sto} \times \eta_{orc} \quad (1)$$

where W_{gen}, W_{comp} are the power generated by the ORC and the power consumed by the compressor of the HP respectively. Q_{sto} denotes the heat transfer rate of the storage tank in the charging process and η_{sto} represents the storage efficiency. *COP* is the coefficient of performance of the HP and η_{orc} is the thermal efficiency of the ORC. As illustrated in Eq. (1), to obtain a higher value of the η_{rt}, it is beneficial to improve the *COP*, η_{orc}, or η_{sto} as much as possible. In this paper, the value of η_{sto} is considered to be 1 as listed in Table 1 for simplicity. Besides the thermodynamic first efficiency, the second efficiency is proposed to evaluate the energy conversion extent. The Lorenz efficiency [36] of HP and exergy efficiency [49] of ORC could be calculated respectively by:

$$\eta_{Lor} = COP/COP_{Lor} = COP/\left[\overline{T}_{sink,hp}/\left(\overline{T}_{sink,hp} - \overline{T}_{source,hp}\right)\right] \quad (2)$$

$$\eta_{e,orc} = W_{gen}/\left[\eta_{sto} Q_{sto}\left(1 - T_{amb}/T_{ave,orc}\right)\right] \quad (3)$$

where COP_{Lor} is the maximum obtainable *COP* of a Lorenz cycle calculated from the thermodynamic average temperatures of the heat source $\overline{T}_{source,hp}$ and heat sink $\overline{T}_{sink,hp}$. The $T_{ave,orc}$ represents the average temperature of the heat source of ORC which can be calculated as follows:

$$T_{ave,orc} = \left(T_{in,hs} - T_{out,hs}\right)/ln\left(T_{in,hs}/T_{out,hs}\right) \quad (4)$$

In addition to the thermodynamic performance evaluation, economic performance assessment is also an important aspect for estimating the TI-PTES system's application potential, which has been involved extensively in former studies [5,6,14]. In this paper, the levelized specific cost of heat c_h and the payback time PBT_{hp} [36] are utilized as the HP system economic performance indicators. Similarly, the electricity production cost EPC_{orc} [50] and the payback time PBT_{orc} [51] are selected for the ORC system. Corresponding definitions are introduced and detailed as follows.

The levelized specific cost of heat c_h and payback time PBT_{hp} are selected as the HP system economic indicators. For the purpose of cost

Table 3
HP system economic parameters and the corresponding formulas.

Parameter	Description	Formula	Ref.
PEC_{eva}, PEC_{cond}, and PEC_{comp}	PEC[a] of the evaporator, condenser and compressor	$PEC_{eva} = 15526 \times (A_{eva}/42)^{0.8}$ $PEC_{cond} = 15526 \times (A_{cond}/42)^{0.8}$ $PEC_{comp} = 19850 \times \left(V_{comp}/279.8 \cdot \eta_{v,comp}\right)^{0.73}$	[52]
PEC_{total}	*PEC* of the main components	$PEC_{total} = PEC_{eva} + PEC_{cond} + PEC_{comp}$	
CRF	capital recovery factor	$CRF = i_{eff}\left(1 + i_{eff}\right)^{n_{lt}}/\left(\left(1 + i_{eff}\right)^{n_{lt}} - 1\right)$	
CF_{TCI}		$CF_{TCI} = CRF \times TCI$	
CF_{OM}	CF[b] of the total capital investment, the OM[c], the heat source energy consumption, and the electricity consumption	$CF_{OM} = f_{OM} \times TCI \times CRF$	[36,53]
CF_{hs}		$CF_{hs} = Q_{eva} \times c_{hs} \times t_{ave}$	
CF_{el}		$CF_{el} = W_{comp} \times c_{el} \times t_{ave}$	
CF_c	CF of the heat supply	$CF_c = Q_{cond} \times \eta_c \times t_{ave} \times c_c$	
c_h	levelized specific cost of heat	$c_h = (CF_{TCI} + CF_{OM} + CF_{hs} + CF_{el})/(Q_{cond} \cdot t_{op,ave})$	
PBT_{hp}	payback time	$PBT_{hp} = TCI/(CF_c - CF_{el} - CF_h)$	

[a] Purchased equipment cost.
[b] Annual cash flow.
[c] Operation and Maintenance cost, which is ignored in this paper.

Table 4
Cost formulas of the ORC components.

Component	Carbon steel material purchasing cost, C_p	Basic material cost, C_{BM}	Actual cost, $C_{BM,2020}$
Heat exchangers Pumps or turbine	$\log C_p = K_1 + K_2 \log_{10}(A) + K_3 [\log_{10}(A)]^2$ $\log C_p = K_1 + K_2 \log_{10}(W) + K_3 [\log_{10}(W)]^2$	$C_{BM} = C_p (B_1 + B_2 F_m F_p)$	$C_{BM,2020} = C_{BM,2001} \cdot CEPCI_{2020} / CEPCI_{2001}$

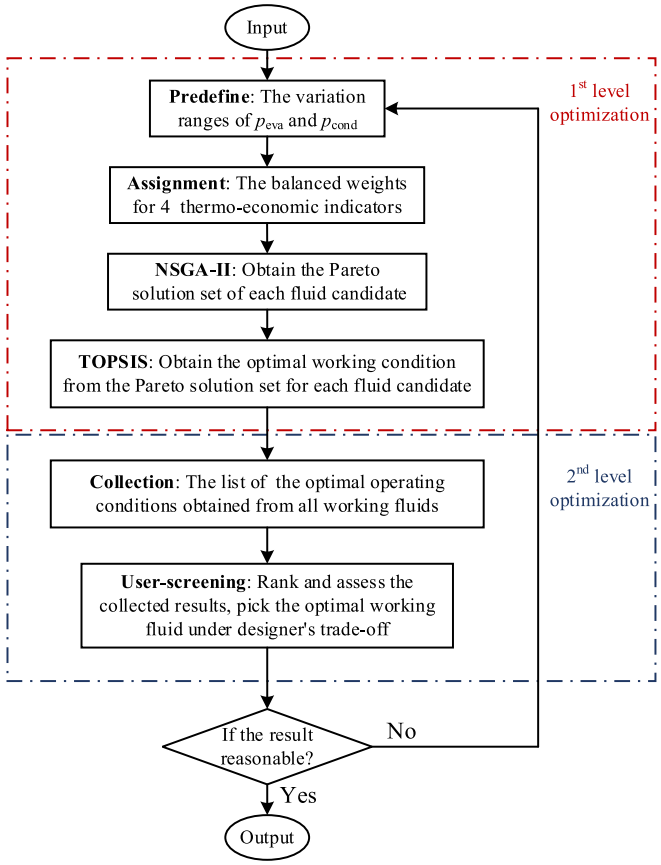

Fig. 2. The double-layer optimization strategy workflow.

analysis, the total capital investment *TCI* mainly includes the following parts: the purchased equipment, assembly, installation, start-up, and other related expenses. Considering the complexity of calculating the *TCI*, a simplified definition is utilized as follows:

$$TCI = f_{TCI} \times PEC_{total} \tag{5}$$

where f_{TCI} is a factor to account for all the expenses and is assumed to be 4 [36]; PEC_{total} represents the main purchased equipment cost consisting of the expenses of the compressor and the heat exchangers, detailed expressions are listed in Table 3.

Besides the one-time investments, the annual cash flows covering the incomes and expenses are considered from 5 aspects: the income from the heat supply and the expenses from the total capital investment, the operation and maintenance, the heat source energy consumption, and the electricity consumption, which are detailed in Table 3. And given the abovementioned expenses, the levelized specific cost of heat c_h and payback time PBT_{hp} then can be calculated and obtained respectively for economic analysis.

The electricity production cost EPC_{orc} and the payback time PBT_{orc} are selected as the ORC system economic indicators. The total purchase cost (C_{total}) comprises the costs associated with the evaporator, turbine, condenser, and working fluid pump. It is roughly estimated by:

$$C_{total} = C_{BM,eva} + C_{BM,turb} + C_{BM,cond} + C_{BM,pump} \tag{6}$$

where the cost expressions of the abovementioned 4 main components are given in Table 4.

Thus, the EPC_{orc} is defined below:

$$EPC_{orc} = \frac{C_{total} CRF + COM}{t_{op} W_{net}} \tag{7}$$

where *CRF* is the capital recovery factor set to 8.02%, *COM* refers to the system operation cost defined as 1.5% of the total system purchase cost, t_{op} represents the system annual operating time set to 8000 h in this study.

The payback time PBT_{orc} is calculated as follows:

$$PBT_{orc} = -\frac{ln\left(1 - i_{eff} C_{total} / C_{n0}\right)}{ln\left(1 + i_{eff}\right)}$$

$$C_{n0} = c_{el} W_{gen} t_{op} - f_{mo} C_{total}$$

where i_{eff} is the effective interest rate with a value of 5% and f_{mo} is the maintenance and operation cost factor with a value of 1.5% [51]. c_{el} is the electricity price set as 0.10 €/kWh [36].

2.2. Optimization methods

It is well known that there is a contradiction between the thermodynamic performance and the economic performance in the TI-PTES system. Therefore, four-objective optimization considering the thermodynamic and economic performance is conducted in this study to evaluate the application potential for each working fluid candidate in HP or ORC. As the initial boundary condition, the pre-assigned system parameters listed in Table 1 remain constant during all the optimization procedures. Evaporation and condensation pressures are decision variables optimized to maximize thermodynamic efficiencies and minimize economic performance indicators of HP or ORC, as illustrated below:

$$\begin{cases} max/min\{y_1(X), y_2(X), y_3(X), y_4(X)\}, X \in [lb, ub] \\ y_1(X) = COP \text{or} \eta_{orc} \\ y_2(X) = \eta_{Lor} \text{or} \eta_{e,orc} \\ y_3(X) = c_h \text{or} EPC_{orc} \\ y_4(X) = PBT_{hp} \text{or} PBT_{orc} \end{cases} \tag{8}$$

where *X* represents the decision variables of HP or ORC, *lb* and *ub* represent the related variation lower and upper bounds of decision variables, which are defined according to the range of specific supercritical temperature of each sort of working fluid.

In this study, the four-objective optimization is conducted by the Non-dominated Sorting Genetic Algorithm (NSGA-II). The population and maximum generation are set as 50 and 300 respectively according to Ref. [17]. In order to select a proper representation among the 50 points on the Pareto front, the TOPSIS (Technique for Order Preference by Similarity to an Ideal Solution) analysis method is adapted and a balanced weight is applied [54]. Thus, an optimized working fluid composition would be obtained through the first-level optimization process as illustrated in Fig. 2. In this paper, the four-objective optimization is arranged as the precondition of the user-defined single-objective working fluid screening process which further focuses on screening fluids under the designer's trade-off in the second level optimization procedure. By varying the weighting factors among the 4 thermo-economic indicators, the fluid candidates would be ranked and screened under various emphasis extents on the thermodynamic or economic aspects in the second-level optimization process. And the user-defined single-objective functions will be defined and detailed in the subsequent section 3.2.

Table 5
Results of model validation.

Parameters	References [36, 49]	Present work	Relative error
ORC:			
m (kg/s)	2.810	2.8096	0.014%
Q_e (kJ/s)	690.254	690.2588	0.0007%
W_t (kW)	85.342	85.32	0.026%
W_{net} (kW)	80.986	80.89	0.119%
η_t (%)	11.73	11.72	0.085%
HP:			
p_{evap} (bar)	4.6	4.6	0
p_{cond} (bar)	18.5	18.5	0
COP (−)	4.4	4.438	0.86%
PBT (years)	4.9	4.928	0.57%
c_h (€/MWh)	32.2	32.165	0.11%

Table 6
Performance indicators for selected fluids of HP.

Medium	COP -	η_{Lor} %	c_h €/MWh	PBT_{hp} years
R717	5.20	39.80	28.12	5.34
Dimethyl ether	5.08	38.89	36.64	10.40
Hexane	5.00	38.28	25.29	3.30
R601	4.99	38.19	24.14	2.56
R1224yd(Z)	4.74	36.28	25.94	3.19
R1234ze(E)	4.67	35.73	90.10	46.07
R600a	4.56	34.87	35.94	9.66
R600	4.55	34.85	26.67	3.25
R1243zf	4.51	34.52	136.60	80.00
R1336mzz(Z)	4.40	33.66	25.95	2.31
Heptane	4.28	32.74	32.75	7.03
R1233zd(E)	4.00	30.56	28.46	2.84
Diethyl ether	3.84	29.40	30.74	4.20
R601a	3.60	27.53	30.55	2.81
R1234ze(Z)	3.43	26.29	31.29	2.49

2.3. Model validation

To validate the thermo-economic modeling of the HP and ORC respectively, the simulated data obtained in this paper has been compared with that published in former studies of Zühlsdorf et al. [36] and H. Xi et al. [49]. The calculated results under the same boundary conditions with former studies are listed in Table 5. From the relative errors in predicting thermodynamic parameters between the former studies and the present work, it can be seen that both the ORC and HP are simulated with a relative error under 1%. Therefore, the accuracy of the models was validated to be satisfactory.

2.4. Boundary conditions

In this study, screening of working fluid pairs in TI-PTES is conducted for the industry low-grade waste heat recovery application situation which assumes the temperature and load of the heat source keep no change as listed in Table 1. The temperature range of industry waste heat covers mostly from 353.15 K to 393.15 K such as 360.85 K [37], 363.15 K [38], 368.15 K [39], 373.15 K [30], and 393.15 K [40] published in former studies. Hence, the inlet temperature of waste heat is initially supposed to be 373.15 K for a typical analysis. Screening suitable working fluid pairs is focused and the performance comparison is addressed among various fluid candidates. Hence, the actual energy storage duration is not considered rather the heat source load for both HP and ORC is assumed to be 3 MW in this study.

To investigate the influence of the heat storage temperature T_{sto}, 7 levels of the T_{sto} are set from 393.15 K to 423.15 K with an increment of 5 K. In addition, the temperature level of the cold tank as shown in Fig. 1 is fixed at 373.15 K no matter which level the hot tank temperature reaches. The study is carried out to explore the capability of the potential working fluid candidates for the TI-PTES system to strengthen its thermo-economic performance, and then offer a referential recommendation for working fluid pair selection under the designer's technical and economic consideration and trade-off.

Table 7
Performance indicators for selected fluids of ORC.

Medium	η_{orc} %	$\eta_{e,orc}$ %	EPC €/MWh	PBT_{orc} years
R1234ze(Z)	10.54	65.57	149.38	19.84
R1233zd(E)	10.47	65.14	108.34	11.44
R152a	10.28	63.93	149.67	19.91
R600	10.26	63.78	149.61	19.89
R245fa	9.94	61.84	94.49	9.38
R123	9.80	60.97	75.56	6.94
R1234ze(E)	9.48	58.96	108.27	11.43
R161	9.40	58.45	101.70	10.42
R1336mzz(Z)	9.32	57.93	68.38	6.11
R601a	9.29	57.76	139.02	17.28
R1224yd(Z)	9.24	57.47	111.36	11.93
R601	9.18	57.07	132.47	15.85
R1243zf	9.10	56.57	149.69	19.92
R600a	9.05	56.28	91.96	9.03
R134a	9.02	56.12	135.04	16.40

3. Results and discussion

3.1. Influence of fluid selection strategy and storage temperature in η_{rt}

Firstly, under a fixed energy storage temperature of 408.15 K, three types of working fluid combination strategies are compared, which are the single pure fluid strategy (SPFS), different pure fluids strategy (DPFS), and different fluids strategy (DFS) considering zeotropic fluids. The top 15 sorts of pure fluids in HP and ORC are listed in Table 6 and Table 7 according to the highest thermodynamic first efficiency. For the highest round-trip efficiency utilizing the SPFS and DPFS strategies, a ranking of 8 sorts of fluid combinations is displayed in Fig. 3.

It can be seen that the highest η_{rt} achieved by SPFS is 46.7% utilizing R600 and the highest η_{rt} achieved by DPFS is 54.8% applying the combination of R717 and R1234ze(Z). Hence based on SPFS, the improvement of the highest η_{rt} is 17.4% through DPFS which is displayed as the difference in performance in Fig. 3. From the remaining

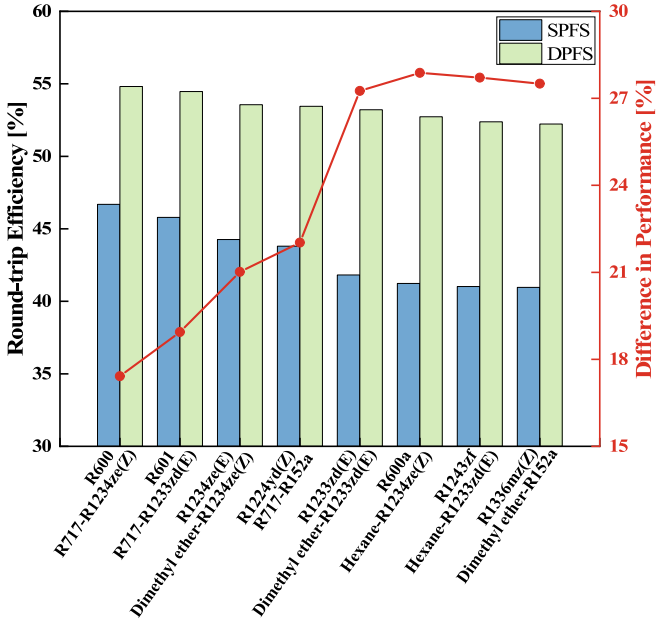

Fig. 3. Eight combinations with the highest round-trip efficiency by SPFS and DPFS.

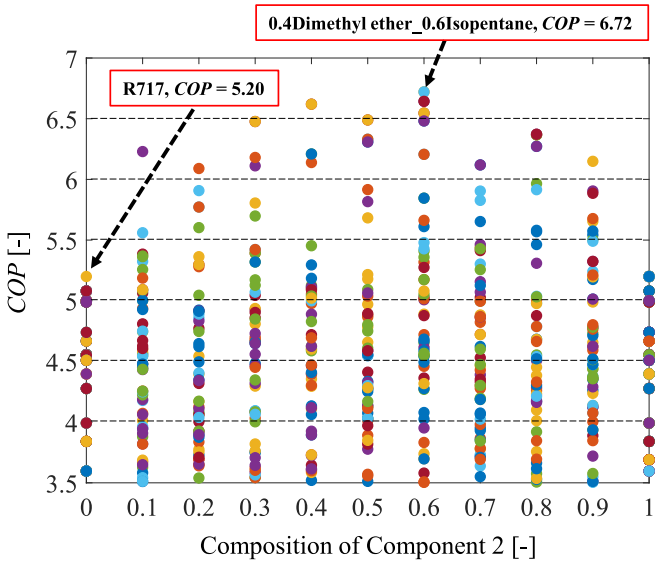

Fig. 4. Screening results of HP.

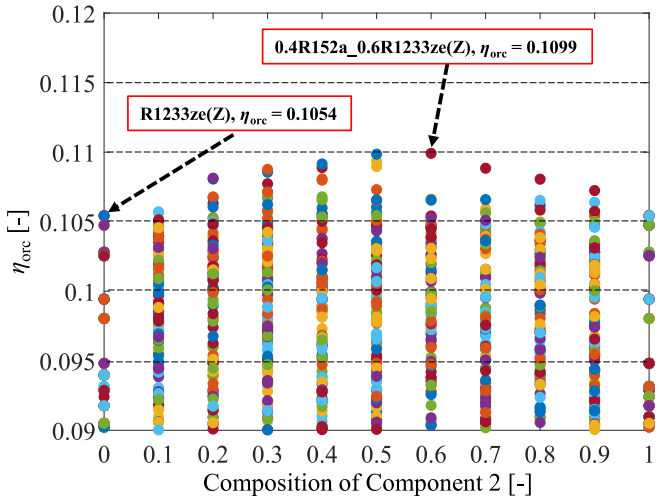

Fig. 5. Screening results of ORC.

rear 7 groups of combination strategy comparisons, the decreasing trend of η_{rt} achieved by DPFS is slower than that achieved by SPFS, which leads to the large difference in performance in the last 3 groups of fluid combinations. This is because the properties of the same kind of working fluid may not be always proper for both HP and ORC at the same time. As listed in Table 6 and Table 7, even though R1234ze(Z) ranks at the top of ORC fluid candidates it is the worst among the top 15 fluids for HP. A similar condition happens to R1233zd(E) and R1224yd(Z) as shown in Fig. 3. Hence, DPFS could make more use of the potential of pure working fluids than traditional SPFS by selecting more suitable working fluids for HP and ORC in a certain range of working fluid candidates.

In order to investigate the effect of another remaining strategy DFS, part relatively superior screening results in scatter figure form of HP and ORC containing the zeotropic fluids are displayed in Fig. 4 and Fig. 5 respectively with only the maximum results marked. And as the supplements for results displayed in Fig. 4 and Fig. 5, the top ten screening results (including strategies SPFS and DFS) for HP and ORC are detailed in Table 8 and Table 9 respectively. It is convenient to compare the maximum *COP* of HP through pure fluids or zeotropic fluids in Fig. 4. On the basis of the application of pure fluid which achieves *COP* = 5.20 by R717, the maximum *COP* is increased to 6.72 by the zeotropic fluid

Table 8
Top ten screening results of HP.

Strategy	Top 10 working fluids	p_{eva} (bar)	p_{cond} (bar)	*COP*
DFS	0.4DME_0.6R601a	10.69	24.27	6.72
	0.4DME_0.6DEE	10.52	24.53	6.64
	0.2DME_0.8DEE	6.91	18.08	6.37
	0.2R290_0.8DEE	7.81	19.45	6.36
	0.5DEE_0.5R1234ze(E)	8.09	20.84	6.33
	0.2R1270_0.8R601a	7.87	19.60	6.27
	0.9R600_0.1Heptane	8.25	20.48	6.23
	0.6R601a_0.4R1243zf	8.20	20.67	6.21
	0.4DEE_0.6R1234ze(E)	9.49	24.10	6.20
	0.1R1270_0.9R1336mzz(Z)	8.89	22.31	6.15
SPFS	R717	37.10	94.91	5.20
	DME	20.10	50.48	5.08
	Hexane	1.16	5.84	5.00
	R601	3.07	12.09	4.99
	R1224yd(Z)	6.07	22.36	4.74
	R1234ze(E)	18.01	47.23	4.67
	R600a	11.41	33.92	4.56
	R600	8.24	27.62	4.55
	R1243zf	19.88	49.59	4.51
	R1336mzz(Z)	3.42	18.41	4.40

Table 9
Top ten screening results of ORC.

Strategy	Top 10 working fluids	p_{eva} (bar)	p_{cond} (bar)	η_{orc} (%)
DFS	0.4R152a_0.6R1234ze(Z)	27.42	4.57	10.991
	0.5R152a_0.5R1233zd(E)	30.07	5.01	10.985
	0.5R152a_0.5R123	29.78	4.99	10.932
	0.6R152a_0.4R1233zd(E)	32.04	5.63	10.915
	0.5R152a_0.5R1224yd(Z)	31.94	5.40	10.896
	0.6R152a_0.4R1234ze(Z)	32.56	5.78	10.889
	0.3R152a_0.7R1234ze(Z)	24.70	4.12	10.884
	0.7R152a_0.3R1336mzz(Z)	34.89	6.00	10.876
	0.7R152a_0.3R1233zd(E)	35.14	6.37	10.856
	0.6R123_0.4R600a	18.91	3.17	10.807
SPFS	R1234ze(Z)	15.40	2.68	10.542
	R1233zd(E)	11.83	1.97	10.474
	R152a	40.65	8.77	10.280
	R600	17.28	3.45	10.255
	R245fa	13.52	2.26	9.943
	R123	8.79	1.68	9.804
	R1234ze(E)	32.47	7.02	9.481
	R161	44.61	12.92	9.399
	R1336mzz(Z)	7.65	1.27	9.315
	R601a	6.76	1.34	9.287

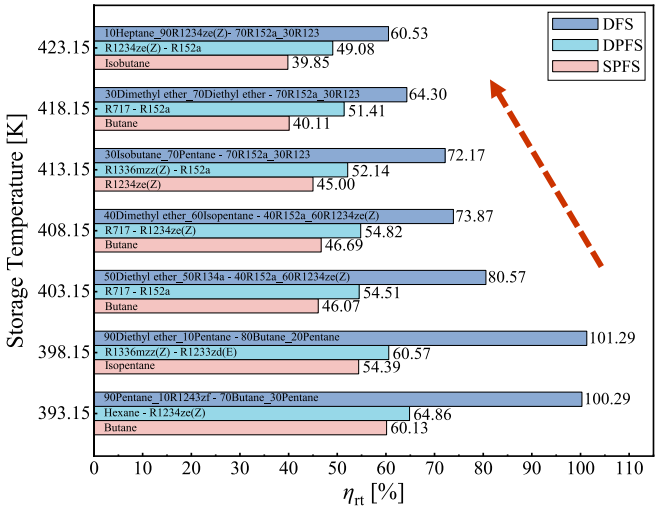

Fig. 6. Screening results under different storage temperatures.

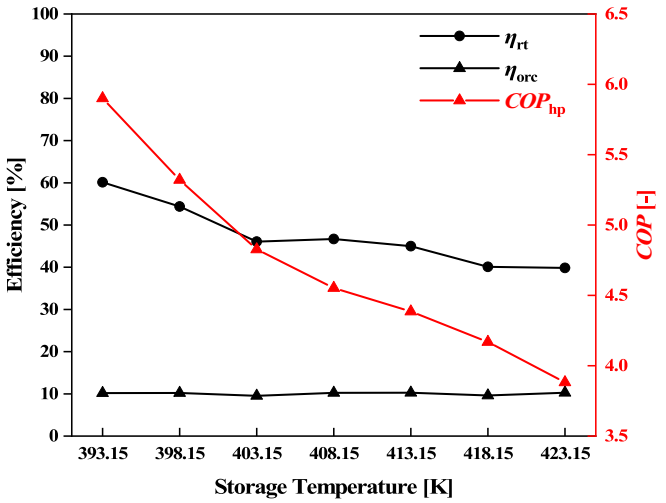

Fig. 7. Efficiencies of Butane under different storage temperatures.

composition of 0.4Dimethyl ether_0.6Isopentane. As for the screening results of ORC in Fig. 5, the maximum η_{orc} of 0.1054 is realized by pure fluid R1233ze(Z) and that of 0.1099 is achieved by zeotropic fluid composition of 0.4R152a_0.6R1233ze(Z). As a result, under a fixed energy storage temperature of 408.15 K, the highest round-trip efficiency by DFS reaches 73.9% which is a great enhancement upon the other two strategies. Based on SPFS, the improvement of the highest η_{rt} is 58.2% through DFS from 46.7% to 73.9%.

As previously mentioned, the influence of working fluid selection strategies in round-trip efficiency is discussed under a fixed energy storage temperature. To further investigate the effect of energy storage temperatures on the efficiency of TI-PTES, optimal screening results under 7 predefined storage temperatures are displayed in Fig. 6. In terms of the overall variation trend of efficiency, with the increase of storage temperature the round-trip efficiency would gradually drop no matter under which fluid selection strategy. However, the decrease trend is not strictly monotonical such as the efficiencies under 393.15 K and 398.15 K through DFS are 100.29% and 101.29%. This is due to the realistic performance behaviors of different working fluid pairs in TI-PTES being optimized under different storage temperatures and the influencing factors include both the storage temperature and the type of the working fluid. What is certain is that no matter under which storage temperature, the efficiency decreases under fluid selection strategies DFS, DPFS, and SPFS in sequence. It is recommended to utilize zeotropic working fluids under relatively low storage temperatures for round-trip efficiency enhancement.

Furthermore, an investigation about the effect of energy storage temperature on the round-trip efficiency is carried out. The pure fluid butane which shows the best performance under SPFS in Fig. 6 is chosen to eliminate the influence of working fluid type in TI-PTES. As shown in Fig. 7, with the increase of storage temperature, the variation trend of round-trip efficiency is decreasing except from 403.15 K to 408.15 K. Referring to Eq. (1), this is because of the enhancement effect by the increment of η_{orc} is slightly stronger than the weakening effect by the decrease of *COP* from 403.15 K to 408.15 K. In general, the fluctuation of η_{orc} is not significant which doesn't agree well with former studies [10,55]. Ideally, the η_{orc} would increase as the storage temperature gets higher. However, the TOPSIS process is adopted in this paper to pick the representative working parameters with balanced thermos-economic performance while evaluating the working fluid, which leads to the irregular variation of η_{orc}. On the other hand, even if under the influence of the TOPSIS process, the decreasing trend of the *COP* is still very clear as shown in Fig. 7, which dominates the general dropping variation pattern of round-trip efficiency. Hence, a higher round-trip efficiency is mainly achieved through a relatively low storage temperature offering a high *COP* in the charging process. A similar statement that the round-trip efficiency η_{rt} is primarily influenced by the *COP* has also been mentioned recently in the research by Qiao et al. [24].

3.2. Two-layer optimization of the working fluid pair selection

As described above, the influence factors of round-trip efficiency are discussed regardless of other performance parameters. To evaluate the integrated performance of TI-PTES, other thermodynamic and economic indicators are considered meanwhile here. In this paper, a two-layer

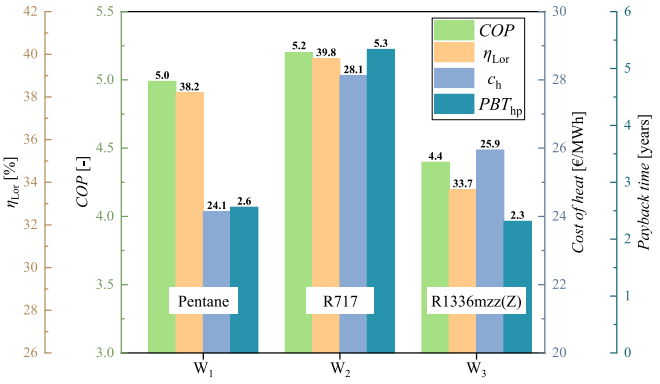

Fig. 9. Screening results of HP under different weighting factors.

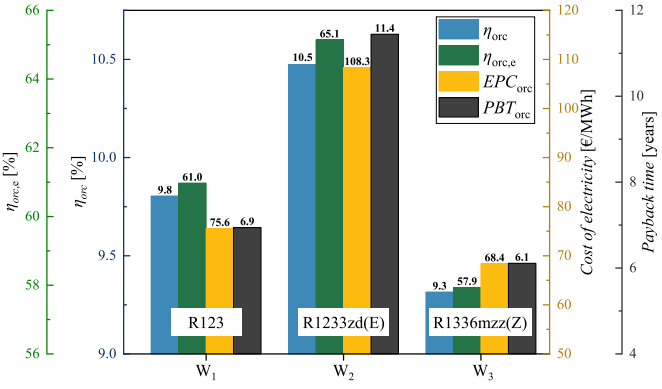

Fig. 10. Screening results of ORC under different weighting factors.

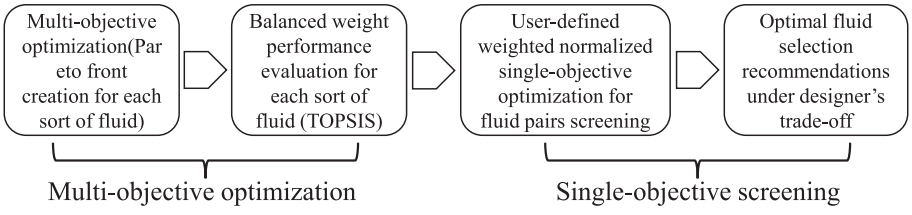

Fig. 8. Two-layer optimization methodology flow of working fluid pair selection.

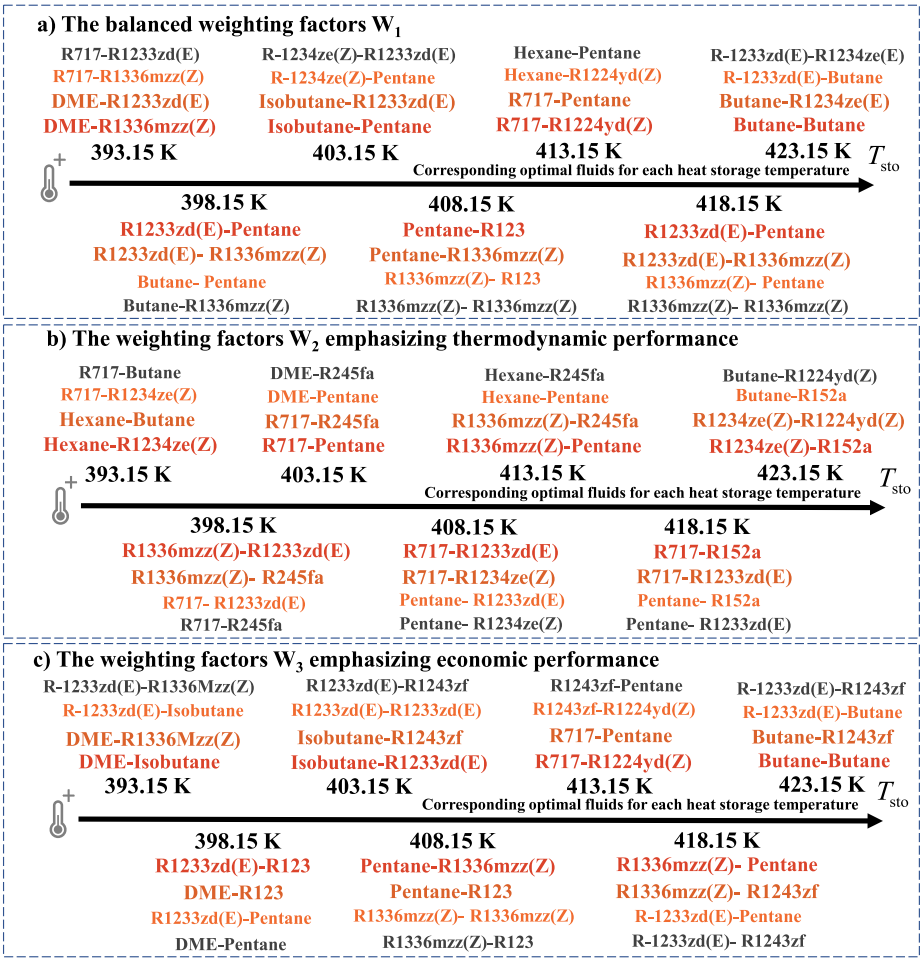

Fig. 11. Pure working fluid pairs recommendations.

fluid pair selection workflow is proposed as shown in Fig. 8. In the first layer, the multi-objective optimization is conducted to get the representation of a specific fluid composition's integrated performance based on NSGA-II algorithm and TOPSIS analysis method. Then, in the second layer, a user-defined evaluation function is proposed similar to Ref. [27]. Through normalized mathematical treatment, single-objective optimization functions are defined for HP and ORC respectively as expressed below. By utilizing a group of weighting factors of which the sum is 1, the performance indicators of each working fluid pair are normalized to a dimensionless value no >1. This dimensionless indicator named *Score* represents the degree of closeness between the actual performance of a certain working fluid pair and the ideal optimal performance under a specific group of weighting factors. Obviously, the range of the *Score* is between 0 and 1 and the higher the *Score* a fluid pair gets, the more suitable it is for the TI-PTES system.

$$Score_{\mathrm{hp}} = w_1\frac{COP}{COP_{\max}} + w_2\frac{\eta_{\mathrm{Lor}}}{\eta_{\mathrm{Lor},max}} + w_3\frac{c_{\mathrm{h},min}}{c_{\mathrm{h}}} + w_4\frac{PBT_{\mathrm{hp},min}}{PBT_{\mathrm{hp}}} \tag{9}$$

$$Score_{\mathrm{orc}} = w_1\frac{\eta_{\mathrm{orc}}}{\eta_{\mathrm{orc},max}} + w_2\frac{\eta_{\mathrm{e,orc}}}{\eta_{\mathrm{e,orc},max}} + w_3\frac{EPC_{\mathrm{orc},min}}{EPC_{\mathrm{orc}}} + w_4\frac{PBT_{\mathrm{orc},min}}{PBT_{\mathrm{orc}}} \tag{10}$$

where the subscript max or min means the maximum or minimum value of the performance indicators such as those listed in Table 6 and Table 7. After the first layer optimization and analysis focusing specifically on η_{rt} has been discussed, in this part the investigation of designing trade-off between 4 thermodynamic and economic performance indicators is performed by ranking the score of normalized single-objective optimization function.

In order to compare the performance differences among the screened working fluids under different thermo-economic designing trade-offs, three groups of weighting factors are utilized similar to Ref. [27]. The first group W_1 regards the four objective functions equally with a balanced weighting factor $[0.25, 0.25, 0.25, 0.25]^{\mathrm{T}}$. Paying more attention on the thermodynamic performance aspect, the second group W_2 is assigned the weighting factors among the four objective functions of $[0.45, 0.45, 0.05, 0.05]^{\mathrm{T}}$. Similarly, emphasizing the economic performance aspect, the third group W_3 is assigned the weighting factors of $[0.05, 0.05, 0.45, 0.45]^{\mathrm{T}}$. The screening results of HP and ORC under different thermo-economic performance weighting factors are shown in Fig. 9 and Fig. 10.

The corresponding normalized objective function value of each kind of fluid is applied as the ranking reference, thus the optimal recommended working fluids with different design weights are obtained respectively. As exhibited in Fig. 9, the optimal fluids under design weights W_1, W_2, and W3 are Pentane, R717 and R1336mzz(Z) respectively. Through the comparison of thermodynamic performance indicators among three design weights, it is obvious that the variation pattern of *COP* and η_{Lor} agrees well with the adjustment of weighting factors. On the basis of balanced weighting factors W_1, the emphasis on the thermodynamic performance by W_2 or weakening it by W_3 causes the increase or decrease of *COP* and η_{Lor} respectively. A similar trend is observed for the economic performance indicators between W_1 and W_2. However, compared with Pentane under W_1, the c_{h} of R1336mzz(Z) under W_3 is slightly higher, which means worse economic performance. With the authors' careful verification, it is found that under the weighting factors W_3, the normalized single-objective optimization

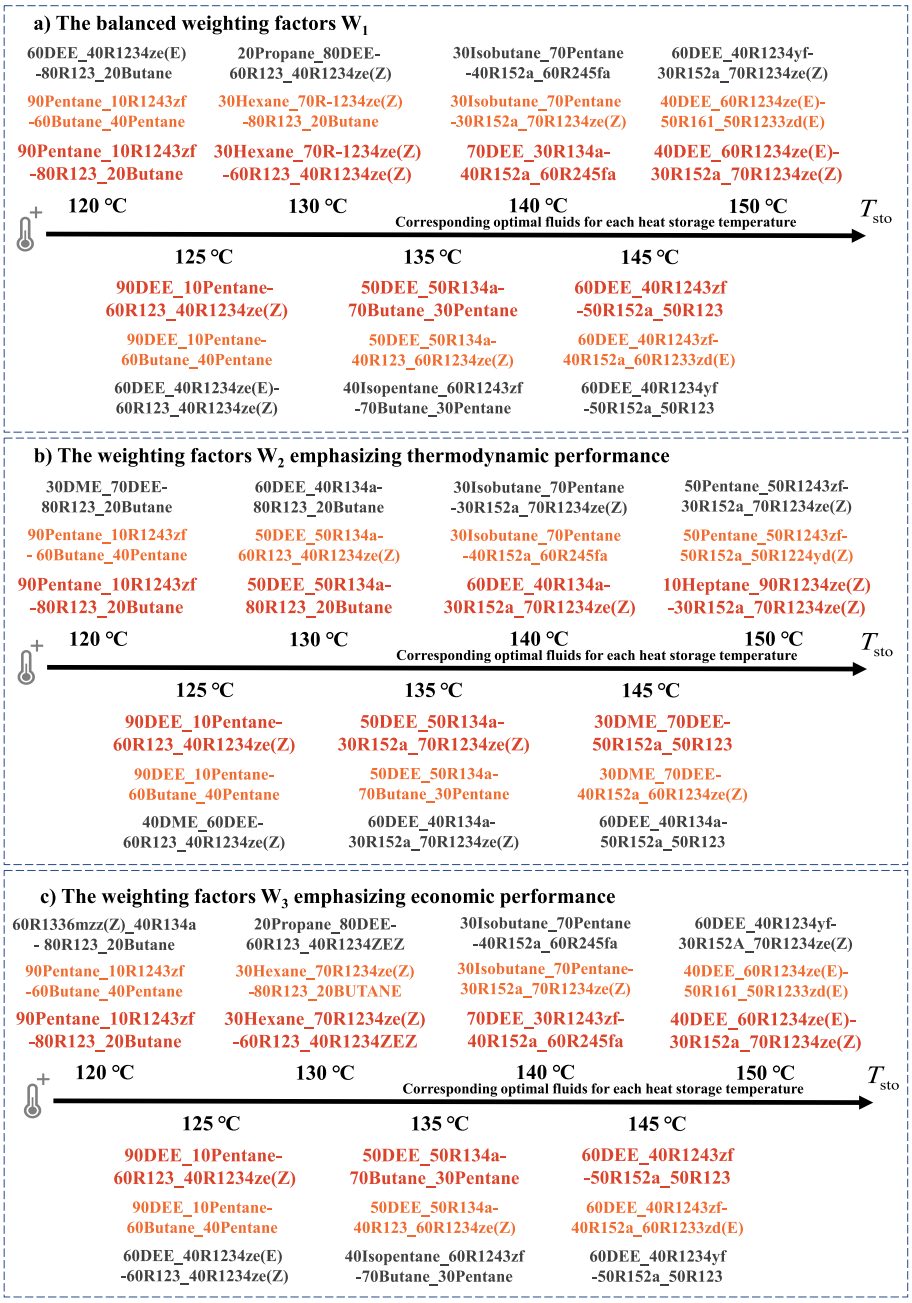

Fig. 12. Zeotropic working fluid pairs recommendations.

function scores obtained by R1336mzz(Z) and Pentane are very close to each other, which means Pentane also behaves excellent under the designing weighting factors W_3 as the second optimal fluid.

Similar to the discussion about screening results of HP above, a more regular variation pattern is found concerning fluid screening of ORC. As exhibited in Fig. 10, the optimal fluids under design weighting factors W_1, W_2, and W_3 are R123, R1233zd(E) and R1336mzz(Z) respectively. With the emphasis on thermodynamic or economic performance, corresponding indicators of optimal fluids vary convincingly as expected. As a result, R1233zd(E) achieves excellent thermodynamic performance, and outstanding economic performance is gained by R1336mzz (Z). Therefore, optimal working fluids can be screened with different thermo-economic trade-offs through the adjustment of corresponding designing weighting factors.

3.3. Working fluid pair selection recommendations under various energy storage temperatures

On the basis of the two-layer screening method, working fluid pair selection recommendations are provided in this paper. Under 7 energy storage temperatures and 3 groups of designing weighting factors, working fluid pairs recommendations of pure and zeotropic types are illustrated in Fig. 11 and Fig. 12. As shown in Fig. 11, the most recommended pure fluid pair is placed approaching the label of each storage temperature, and it is in the dark red in the picture. In other words, the pure working fluid pair painted in a duller color type refers to a subsequent recommendation. Hence, at storage temperature 408.15 K, the recommended pure working fluid pairs listed in order of balanced thermo-economic performance are [Pentane-R123], [Pentane-R1336mzz(Z)], [R1336mzz(*Z*)-R123], and [R1336mzz(Z)-R1336mzz (Z)] respectively. The former pure fluid of each pair refers to the

Table 10
Environmental and safety properties of working fluid candidates.

Working fluid	Subsystem	GWP	ODP	SG
R50	HP	29.8	0	A3
R170	HP	2.9	0	A3
R1150	HP	20	0	A3
DME	HP	1	0	A3
Hexane	HP	3.06	0.0001	B2
Heptane	HP	3	0.22	B2
R717	HP	0	0	B2L
R718	HP	0.2	0	A1
R744	HP	1	0	A1
DEE	HP	4	0	A3
R134a	HP/ORC	1300	0	A1
R1270	HP/ORC	3.1	0	A3
R290	HP/ORC	3	0	A3
R600	HP/ORC	3	0	A3
R600a	HP/ORC	3	0	A3
R601	HP/ORC	4	0	A3
R601a	HP/ORC	4	0	A3
R1224yd(Z)	HP/ORC	<1	0.00012	A1
R1233zd(E)	HP/ORC	1	0.00034	A1
R1234ze(E)	HP/ORC	6	0	A2L
R1234ze(Z)	HP/ORC	<10	0	A2L
R1234yf	HP/ORC	1	0	A2L
R1243zf	HP/ORC	4	0	A2
R1336mzz(Z)	HP/ORC	2	0	A1
R161	ORC	4	0	A2
R152a	ORC	153	0	A2
R123	ORC	79	0.03	B1
R227ea	ORC	3350	0	A1
R245fa	ORC	858	0	B1
R1123	ORC	3	0	A1
R1216	ORC	17,340	0	A1

Table 11
Comprehensive practical screening results under weighting factor W_1.

Strategy	T_{sto} / K	Optimal working fluid pair	Suboptimal working fluid pair
DPFS	393.15	R1233zd(E) - R1336mzz(Z)	R1224yd(Z) - R1233zd(E)
	398.15	R1233zd(E) - R1336mzz(Z)	R1224yd(Z) - R152a
	403.15	R1234ze(Z) - R1233zd(E)	R1233zd(E) - R1336mzz(Z)
	408.15	R1336mzz(Z) - R1336mzz (Z)	R1233zd(E) - R1233zd(E)
	413.15	R1234ze(Z) - R1224yd(Z)	R1243zf - R1336mzz(Z)
	418.15	R1233zd(E) - R1336mzz(Z)	R1336mzz(Z) - R1243zf
	423.15	R1233zd(E) - R1234ze(E)	R1336mzz(Z) - R1243zf
DFS	393.15	0.6R1336mzz(Z)_0.4R134a - 0.4R152a_0.6R1233zd(E)	0.4R1234ze(E) _0.6R1336mzz(Z) - 0.4R152a_0.6R1224yd(Z)
	398.15	0.3R1243zf_0.7R1336mzz (Z) - 0.4R152a_0.6R1233zd (E)	0.3R1234yf_0.7R1336mzz (Z) - 0.1R134a_0.9R1234ze (Z)
	403.15	0.2R1234yf_0.8R1336mzz (Z) - 0.1R152a_0.9R1234ze (Z)	0.4R1234yf_0.6R1336mzz (Z) - 0.2R152a_0.8R1234ze (Z)
	408.15	0.3R1234ze(E) _0.7R1336mzz(Z) - 0.3R152a_0.7R1234ze(Z)	0.7R1336mzz(Z)_0.3R134a - 0.1R152a_0.9R1234ze(Z)
	413.15	0.3R1234yf_0.7R1336mzz (Z) - 0.3R152a_0.7R1234ze (Z)	0.8R1336mzz(Z)_0.2R134a - 0.6R152a_0.4R1336mzz(Z)
	418.15	0.6R1336mzz(Z)_0.4R134a - 0.4R152a_0.6R1233zd(E)	0.5R1234ze(E) _0.5R1336mzz(Z) - 0.4R152a_0.6R1224yd(Z)
	423.15	0.4R1243zf_0.6R1336mzz (Z) - 0.3R152a_0.7R1234ze (Z)	0.7R1336mzz(Z)_0.3R134a - 0.5R152a_0.5R1224yd(Z)

Table 12
Comprehensive practical screening results under weighting factor W_2.

Strategy	T_{sto} / K	Optimal working fluid pair	Suboptimal working fluid pair
DPFS	393.15	R1224yd(Z) - R1234ze(Z)	R1336mzz(Z) - R1336mzz(Z)
	398.15	R1336mzz(Z) - R1233zd (E)	R1233zd(E) - R1336mzz(Z)
	403.15	R1234ze(Z) - R152a	R1234ze(E) - R1336mzz(Z)
	408.15	R1224yd(Z) - R1233zd(E)	R1336mzz(Z) - R1234ze(Z)
	413.15	R1336mzz(Z) - R1234ze (Z)	R1234ze(Z) - R152a
	418.15	R1233zd(E) - R152a	R1234ze(Z) - R1233zd(E)
	423.15	R1234ze(Z) - R152a	R1234ze(E) - R1224yd(Z)
DFS	393.15	0.7R1336mzz(Z) _0.3R134a - 0.4R152a_0.6R1233zd(E)	0.6R1336mzz(Z)_0.4R134a - 0.5R152a_0.5R1233zd(E)
	398.15	0.7R1336mzz(Z) _0.3R134a - 0.4R152a_0.6R1233zd(E)	0.3R1234yf_0.7R1336mzz(Z) - 0.1R134a_0.9R1234ze(Z)
	403.15	0.7R1336mzz(Z) _0.3R134a - 0.2R152a_0.8R1234ze(Z)	0.6R1336mzz(Z)_0.4R134a - 0.1R152a_0.9R1234ze(Z)
	408.15	0.7R1336mzz(Z) _0.3R134a - 0.3R152a_0.7R1234ze(Z)	0.3R1234ze(E)_0.7R1336mzz (Z) - 0.4R152a_0.6R1234ze(Z)
	413.15	0.6R1336mzz(Z) _0.4R134a - 0.3R152a_0.7R1234ze(Z)	0.8R1336mzz(Z)_0.2R134a - 0.6R152a_0.4R1233zd(E)
	418.15	0.6R1336mzz(Z) _0.4R134a - 0.4R152a_0.6R1234ze(Z)	0.7R1336mzz(Z)_0.3R134a - 0.4R152a_0.6R1233zd(E)
	423.15	0.7R1336mzz(Z) _0.3R134a - 0.3R152a_0.7R1234ze(Z)	0.4R1243zf_0.6R1336mzz(Z) - 0.5R152a_0.5R1224yd(Z)

Table 13
Comprehensive practical screening results under weighting factor W_3.

Strategy	T_{sto} / K	Optimal working fluid pair	Suboptimal working fluid pair
DPFS	393.15	R1233zd(E) - R1336mzz(Z)	R1234ze(Z) - R1233zd(E)
	398.15	R1233zd(E) - R1336mzz(Z)	R1234ze(Z) - R152a
	403.15	R1233zd(E) - R1233zd(E)	R1234ze(Z) - R1243zf
	408.15	R1336mzz(Z) - R1336mzz (Z)	R1224yd(Z) - R1233zd(E)
	413.15	R1243zf - R1224yd(Z)	R1233zd(E) - R1336mzz(Z)
	418.15	R1336mzz(Z) - R1243zf	R1233zd(E) - R1336mzz(Z)
	423.15	R1233zd(E) - R1243zf	R1336mzz(Z) - R1234ze(E)
DFS	393.15	0.6R1336mzz(Z)_0.4R134a - 0.4R152a_0.6R1233zd(E)	0.4R1234ze(E) _0.6R1336mzz(Z) - 0.4R152a_0.6R1224yd(Z)
	398.15	0.3R1243zf_0.7R1336mzz (Z) - 0.4R152a_0.6R1233zd (E)	0.3R1234yf_0.7R1336mzz (Z) - 0.1R134a_0.9R1234ze (Z)
	403.15	0.4R1234yf_0.6R1336mzz (Z) - 0.1R152a_0.9R1234ze (Z)	0.2R1234yf_0.8R1336mzz (Z) - 0.2R152a_0.8R1234ze (Z)
	408.15	0.3R1234ze(E) _0.7R1336mzz(Z) - 0.3R152a_0.7R1234ze(Z)	0.2R1243zf_0.8R1336mzz (Z) - 0.1R152a_0.9R1234ze (Z)
	413.15	0.3R1234yf_0.7R1336mzz (Z) - 0.3R152a_0.7R1234ze (Z)	0.8R1336mzz(Z)_0.2R134a - 0.6R152a_0.4R1336mzz(Z)
	418.15	0.6R1336mzz(Z)_0.4R134a - 0.4R152a_0.6R1233zd(E)	0.5R1234ze(E) _0.5R1336mzz(Z) - 0.4R152a_0.6R1224yd(Z)
	423.15	0.4R1243zf_0.6R1336mzz (Z) - 0.3R152a_0.7R1234ze (Z)	0.7R1336mzz(Z)_0.3R134a - 0.5R152a_0.5R1224yd(Z)

working fluid utilized in HP and the latter one is adopted in ORC. With the change in T_{sto}, the screening results vary at the same time to form a better match between working fluids and working conditions.

The pure fluid pair [Butane-Butane] shows the optimum balanced performance at a storage temperature of 423.15 K, which means under the second layer single-object evaluation criteria, the strategy DPFS is not always prior to SPFS. By comparing the screening results among different designing weighting factors, there is a huge difference between W_1 and W_2 and the screened results have little in common. On the other hand, the outputs under W_1 and W_3 are similar to each other to some

extent. Therefore, with different designing trade-off plans the final screened pure working fluid pairs could be very distinctive.

As recommended above, all the working fluid pairs are screened and ranked according to their thermo-economic performance. However, from the perspective of realistic utilizations in different daily energy storage scenarios (such as the steelworks, chemical plants, thermal power plants and so on), the environmental friendliness, toxicity, and flammability aspects of the working fluids must be taken into consideration. Hence, the ODP (Ozone Depletion Potential) value, GWP (Global Warming Potential) value, and SG (safety grade) of each working fluid candidate have been summarized and listed in Table 10 for further screening of working fluid pairs [41–48].

The subsequent consideration entails the comprehensive evaluation of flammability, toxicity, and environmental compatibility parameters. In this context, fluids exhibiting pronounced flammability or toxicity are categorically deemed unsuitable. By leveraging established knowledge pertaining to the flammability characteristics of specific fluid categories (e.g., alkynes, alkenes, alkanes) and/or toxicity (conforming to ASHRAE Standard 34 classifications B1 and B2), the initial potential fluids can be systematically screened, resulting in a refined selection on the basis of preliminary results listed in Fig. 11. And the best and second comprehensive practical working fluid pairs are listed in Table 11, Table 12, and Table 13, which are categorized by various heat storage temperatures.

By a similar way of listing pure working fluid pairs, recommendations of zeotropic working fluid pairs are displayed in Fig. 12. It can be observed that the fluid composition DEE more or less exists in the HP zeotropic working fluid pairs under the different storage temperatures which agrees well with former study [36,56]. However, DEE has many drawbacks such as flammability, explosive properties and toxicity. Therefore the recommendations of zeotropic working fluid pairs may need to be screened twice if the safety and environmental protection aspects are considered. Other compositions of zeotropic fluid pairs give a relatively good environmentally friendly solution. Similar to the consideration for comprehensive practical screening of pure working fluid pairs, the practical recommendations of zeotropic working fluid pairs are also given in Table 11, Table 12, and Table 13. All the given recommendations are derived under a special thermodynamic boundary condition and proper adjustment should be made for the realistic utilization.

4. Conclusions

With the increasing demand for energy saving, emission reduction and cost reduction, the Thermally Integrated Pumped Thermal Electricity Storage system has been considered a promising electricity storage method for recovering waste heat and shifting electricity costs from on-peak periods to off-peak periods. The system's performance hinges critically on the selection of working fluid pairs and the energy storage temperature. A dual-layer optimization strategy for selecting suitable working fluid pairs has been established. Key findings include:

(1) Three types of fluid pair combination strategies were compared at a fixed energy storage temperature of 408.15 K. The strategy of utilizing different pure fluids for the heat pump and organic Rankine cycles outperformed the single pure fluid strategy, enhancing the highest round-trip efficiency by 17.4%. The adoption of zeotropic fluids further increased thermodynamic efficiency, achieving a 58.2% improvement in the highest round-trip efficiency.

(2) The influence of energy storage temperature in round-trip efficiency was investigated under 7 temperatures from 393.15 K to 423.15 K with equal intervals of 5 K. It was found that no matter under which storage temperature, the round-trip efficiency of TI-PTES decreased under fluid selection strategies DFS, DPFS, and SPFS in sequence. The optimum round-trip efficiency of 101.29% was achieved at 398.15 K, mainly influenced by the enhanced coefficient of performance (COP) in heat pump at a lower storage temperature.

(3) The two-layer optimization approach facilitated a thorough thermo-economic performance evaluation under various weighting factors. Prioritizing either thermodynamic or economic factors proved crucial for effectively screening working fluids, allowing for targeted trade-offs in design considerations.

(4) Through varying energy storage temperature and designing weighting factors, optimal working fluid pair recommendations including pure fluids and zeotropic ones were proposed to give a full-scale solution to the fluid selection of TI-PTES. Variations in storage temperatures and weighting factors influenced the screening outcomes, ensuring an optimal match between working fluids and working conditions.

CRediT authorship contribution statement

Ding Wu: Writing – original draft, Methodology, Formal analysis, Conceptualization. **Bo Ma:** Conceptualization, Methodology, Supervision, Writing – review & editing. **Ji Zhang:** Writing – review & editing, Supervision, Methodology, Funding acquisition, Formal analysis, Conceptualization. **Yanqi Chen:** Writing – review & editing, Formal analysis. **Feifan Shen:** Writing – review & editing, Formal analysis. **Xun Chen:** Writing – review & editing, Formal analysis. **Chuang Wen:** Writing – review & editing, Supervision, Methodology, Formal analysis, Conceptualization. **Yan Yang:** Conceptualization, Formal analysis, Investigation, Methodology, Supervision, Writing – review & editing.

Declaration of competing interest

The authors declare that they have no known competing financial interests or personal relationships that could have appeared to influence the work reported in this paper.

Data availability

Data will be made available on request.

Acknowledgments

The authors gratefully acknowledge the financial support received from the National Key Research and Development Program of China (project ID: 2022YFE0118500) for the research presented in this paper.

References

[1] Lakzian E, Yazdani S, Salmani F, Mahian O, Kim HD, Ghalambaz M, et al. Supersonic separation towards sustainable gas removal and carbon capture. Prog Energy Combust Sci 2024;103:101158. https://doi.org/10.1016/j.pecs.2024.101158.

[2] Grauberger A, Young D, Bandhauer T. Experimental validation of an organic rankine-vapor compression cooling cycle using low GWP refrigerant R1234ze(E). Appl Energy 2022;307:15. https://doi.org/10.1016/j.apenergy.2021.118242.

[3] Oyedepo SO, Fakeye BA. Waste heat recovery technologies: pathway to sustainable energy development. J Therm Eng 2021;7(324–48). https://doi.org/10.18186/thermal.850796.

[4] Nan SB, Zhou M, Li GY. Optimal residential community demand response scheduling in smart grid. Appl Energy 2018;210:1280–9. https://doi.org/10.1016/j.apenergy.2017.06.066.

[5] Hu SZ, Yang Z, Li J, Duan YY. Thermo-economic analysis of the pumped thermal energy storage with thermal integration in different application scenarios. Energy Convers Manag 2021;236:15. https://doi.org/10.1016/j.enconman.2021.114072.

[6] Zhang H, Wang L, Lin XP, Chen HS. Technical and economic analysis of Brayton-cycle-based pumped thermal electricity storage systems with direct and indirect thermal energy storage. Energy 2022;239:19. https://doi.org/10.1016/j.energy.2021.121966.

[7] Liang T, Vecchi A, Knobloch K, Sciacovelli A, Engelbrecht K, Li YL, et al. Key components for Carnot battery: technology review, technical barriers and selection criteria. Renew Sustain Energy Rev 2022;163:23. https://doi.org/10.1016/j.rser.2022.112478.

[8] Mejia C, Kajikawa Y. Emerging topics in energy storage based on a large-scale analysis of academic articles and patents. Appl Energy 2020;263:17. https://doi.org/10.1016/j.apenergy.2020.114625.

[9] Steinmann WD. The CHEST (compressed heat energy STorage) concept for facility scale thermo mechanical energy storage. Energy 2014;69:543–52. https://doi.org/10.1016/j.energy.2014.03.049.

[10] Zhang MY, Shi LF, Hu P, Pei G, Shu GQ. Carnot battery system integrated with low-grade waste heat recovery: toward high energy storage efficiency. J Energy Storage 2023;57:15. https://doi.org/10.1016/j.est.2022.106234.

[11] Dumont O, Lemort V. Mapping of performance of pumped thermal energy storage (Carnot battery) using waste heat recovery. Energy 2020;211:10. https://doi.org/10.1016/j.energy.2020.118963.

[12] Frate GF, Ferrari L, Desideri U. Rankine Carnot batteries with the integration of thermal energy sources: a review. Energies 2020;13:28. https://doi.org/10.3390/en13184766.

[13] Wang PL, Li QB, Liu C, Wang RQ, Luo Z, Zou P, et al. Comparative analysis of system performance of thermally integrated pumped thermal energy storage systems based on organic flash cycle and organic Rankine cycle. Energy Convers Manag 2022;273:17. https://doi.org/10.1016/j.enconman.2022.116416.

[14] Tian WB, Xi H. Comparative analysis and optimization of pumped thermal energy storage systems based on different power cycles. Energy Convers Manag 2022;259:18. https://doi.org/10.1016/j.enconman.2022.115581.

[15] Frate GF, Antonelli M, Desideri U. A novel pumped thermal electricity storage (PTES) system with thermal integration. Appl Therm Eng 2017;121:1051–8. https://doi.org/10.1016/j.applthermaleng.2017.04.127.

[16] Lu C, Shi XP, He Q, Liu YX, An XG, Cui SS, et al. Dynamic modeling and numerical investigation of novel pumped thermal electricity storage system during startup process. J Energy Storage 2022;55:15. https://doi.org/10.1016/j.est.2022.105409.

[17] Fan RX, Xi H. Energy, exergy, economic (3E) analysis, optimization and comparison of different Carnot battery systems for energy storage. Energy Convers Manag 2022;252:14. https://doi.org/10.1016/j.enconman.2021.115037.

[18] Jockenhofer H, Steinmann WD, Bauer D. Detailed numerical investigation of a pumped thermal energy storage with low temperature heat integration. Energy 2018;145:665–76. https://doi.org/10.1016/j.energy.2017.12.087.

[19] Eppinger B, Zigan L, Karl J, Will S. Pumped thermal energy storage with heat pump-ORC-systems: comparison of latent and sensible thermal storages for various fluids. Appl Energy 2020;280:18. https://doi.org/10.1016/j.apenergy.2020.115940.

[20] Eppinger B, Steger D, Regensburger C, Karl J, Schlucker E, Will S. Carnot battery: simulation and design of a reversible heat pump-organic Rankine cycle pilot plant. Appl Energy 2021;288:10. https://doi.org/10.1016/j.apenergy.2021.116650.

[21] Steger D, Regensburger C, Eppinger B, Will S, Karl J, Schlucker E. Design aspects of a reversible heat pump - organic rankine cycle pilot plant for energy storage. Energy 2020;208:8. https://doi.org/10.1016/j.energy.2020.118216.

[22] Ma RQ, Qiao HN, Yu XH, Yang B, Yang H. Thermo-economic analysis and multi-objective optimization of a reversible heat pump-organic Rankine cycle power system for energy storage. Appl Therm Eng 2023;220:13. https://doi.org/10.1016/j.applthermaleng.2022.119658.

[23] Yu XA, Li Z, Zhang ZP, Wang L, Qian G, Huang R, et al. Energy, exergy, economic performance investigation and multi-objective optimization of reversible heat pump-organic Rankine cycle integrating with thermal energy storage. Case Stud Therm Eng 2022;38:16. https://doi.org/10.1016/j.csite.2022.102321.

[24] Qiao H, Yu X, Yang B. Working fluid design and performance optimization for the heat pump-organic Rankine cycle Carnot battery system based on the group contribution method. Energy Convers Manag 2023;293:117459. https://doi.org/10.1016/j.enconman.2023.117459.

[25] Dai R, Tian R, Zheng S, Wei M. Finite-time thermodynamic and economic analysis of Rankine Carnot battery based on life-cycle method. Appl Therm Eng 2023;230:120813. https://doi.org/10.1016/j.applthermaleng.2023.120813.

[26] Zhang M, Shi L, Hu P, Pei G, Shu G. Carnot battery system integrated with low-grade waste heat recovery: toward high energy storage efficiency. J Energy Storage 2023;57:106234. https://doi.org/10.1016/j.est.2022.106234.

[27] Frate GF, Ferrari L, Desideri U. Multi-criteria investigation of a pumped thermal electricity storage (PTES) system with thermal integration and sensible heat storage. Energy Convers Manag 2020;208:24. https://doi.org/10.1016/j.enconman.2020.112530.

[28] Fan RX, Xi H. Exergoeconomic optimization and working fluid comparison of low-temperature Carnot battery systems for energy storage. J Energy Storage 2022;51:15. https://doi.org/10.1016/j.est.2022.104453.

[29] Wang Z, Xia R, Jiang Y, Cao M, Ji Y, Han F. Evaluation and optimization of an engine waste heat assisted Carnot battery system for ocean-going vessels during harbor stays. J Energy Storage 2023;73:108866. https://doi.org/10.1016/j.est.2023.108866.

[30] Hassan AH, O'Donoghue L, Sanchez-Canales V, Corberan JM, Paya J, Jockenhofer H. Thermodynamic analysis of high-temperature pumped thermal energy storage systems: refrigerant selection, performance and limitations. Energy Rep 2020;6:147–59. https://doi.org/10.1016/j.egyr.2020.05.010.

[31] Heberle F, Preissinger M, Bruggemann D. Zeotropic mixtures as working fluids in organic Rankine cycles for low-enthalpy geothermal resources. Renew Energy 2012;37:364–70. https://doi.org/10.1016/j.renene.2011.06.044.

[32] Chys M, van den Broek M, Vanslambrouck B, De Paepe M. Potential of zeotropic mixtures as working fluids in organic Rankine cycles. Energy 2012;44:623–32. https://doi.org/10.1016/j.energy.2012.05.030.

[33] Guo H, Gong MQ, Qin XY. Performance analysis of a modified subcritical zeotropic mixture recuperative high-temperature heat pump. Appl Energy 2019;237:338–52. https://doi.org/10.1016/j.apenergy.2018.12.094.

[34] Bernehed A. ZeoPTES: zeotropic pumped thermal energy storage with an Ammonia-water mixture as working fluid. Energy Technol 2021;9:16. https://doi.org/10.1002/ente.202100470.

[35] Lu P, Luo XL, Wang J, Chen JY, Liang YZ, Yang Z, et al. Thermodynamic analysis and evaluation of a novel composition adjustable Carnot battery under variable operating scenarios. Energy Convers Manag 2022;269:18. https://doi.org/10.1016/j.enconman.2022.116117.

[36] Zuhlsdorf B, Jensen JK, Elmegaard B. Heat pump working fluid selection-economic and thermodynamic comparison of criteria and boundary conditions. Int J Refrig-Rev Int Froid 2019;98:500–13. https://doi.org/10.1016/j.ijrefrig.2018.11.034.

[37] Lee U, Kim K, Han C. Design and optimization of multi-component organic rankine cycle using liquefied natural gas cryogenic exergy. Energy 2014;77:520–32. https://doi.org/10.1016/j.energy.2014.09.036.

[38] Yang B, Jiang Y, Fu L, Zhang SG. Conjugate heat and mass transfer study of a new open-cycle absorption heat pump applied to total heat recovery of flue gas. Appl Therm Eng 2018;138:888–99. https://doi.org/10.1016/j.applthermaleng.2018.04.054.

[39] Hijriawan M, Pambudi NA, Wijayanto DS, Biddinika MK, Saw LH. Experimental analysis of R134a working fluid on organic Rankine cycle (ORC) systems with scroll-expander. Eng Sci Technol 2022;29:6. https://doi.org/10.1016/j.jestch.2021.06.016.

[40] Feng YQ, Hung TC, Greg K, Zhang YN, Li BX, Yang JF. Thermoeconomic comparison between pure and mixture working fluids of organic Rankine cycles (ORCs) for low temperature waste heat recovery. Energy Convers Manag 2015;106:859–72. https://doi.org/10.1016/j.enconman.2015.09.042.

[41] Abedini H, Vieren E, Demeester T, Beyne W, Lecompte S, Quoilin S, et al. A comprehensive analysis of binary mixtures as working fluid in high temperature heat pumps. Energy Convers Manag 2023;277:15. https://doi.org/10.1016/j.enconman.2022.116652.

[42] Wu D, Hu B, Wang RZ. Vapor compression heat pumps with pure low-GWP refrigerants. Renew Sustain Energy Rev 2021;138:20. https://doi.org/10.1016/j.rser.2020.110571.

[43] Yan HZ, Wu D, Liang JY, Hu B, Wang RZ. Selection and validation on low-GWP refrigerants for a water-source heat pump. Appl Therm Eng 2021;193:12. https://doi.org/10.1016/j.applthermaleng.2021.116938.

[44] Iskan U, Direk M. Experimental performance evaluation of the dual-evaporator ejector refrigeration system using environmentally friendly refrigerants of R1234ze(E), ND, R515a, R456a, and R516a as a replacement for R134a. J Clean Prod 2022;352:12. https://doi.org/10.1016/j.jclepro.2022.131612.

[45] Heredia-Aricapa Y, Belman-Flores JM, Mota-Babiloni A, Serrano-Arellano J, Garcia-Pabon JJ. Overview of low GWP mixtures for the replacement of HFC refrigerants: R134a, R404A and R410A. Int J Refrig 2020;111:113–23. https://doi.org/10.1016/j.ijrefrig.2019.11.012.

[46] Gimenez-Prades P, Navarro-Esbri J, Arpagaus C, Fernandez-Moreno A, Mota-Babiloni A. Novel molecules as working fluids for refrigeration, heat pump and organic Rankine cycle systems. Renew Sustain Energy Rev 2022;167:20. https://doi.org/10.1016/j.rser.2022.112549.

[47] Qyyum MA, Khan A, Ali S, Khurram MS, Mao N, Naquash A, et al. Assessment of working fluids, thermal resources and cooling utilities for organic Rankine cycles: state-of-the-art comparison, challenges, commercial status, and future prospects. Energy Convers Manag 2022;252:26. https://doi.org/10.1016/j.enconman.2021.115055.

[48] Xu WC, Zhao RK, Deng S, Zhao L, Mao SS. Is zeotropic working fluid a promising option for organic Rankine cycle: a quantitative evaluation based on literature data. Renew Sustain Energy Rev 2021;148:18. https://doi.org/10.1016/j.rser.2021.111267.

[49] Xi H, Li MJ, Xu C, He YL. Parametric optimization of regenerative organic Rankine cycle (ORC) for low grade waste heat recovery using genetic algorithm. Energy 2013;58:473–82. https://doi.org/10.1016/j.energy.2013.06.039.

[50] Zhang C, Liu C, Wang SK, Xu XX, Li QB. Thermo-economic comparison of subcritical organic Rankine cycle based on different heat exchanger configurations. Energy 2017;123:728–41. https://doi.org/10.1016/j.energy.2017.01.132.

[51] Xia XX, Wang ZQ, Zhou NJ, Hu YH, Zhang JP, Chen Y. Working fluid selection of dual-loop organic Rankine cycle using multi-objective optimization and improved grey relational analysis. Appl Therm Eng 2020;171:115028. https://doi.org/10.1016/j.applthermaleng.2020.115028.

[52] Lu Z, Yao Y, Liu G, Ma W, Gong Y. Thermodynamic and economic analysis of a high temperature Cascade heat pump system for steam generation. Processes 2022:1862. https://doi.org/10.3390/pr10091862.

[53] Bühler F, Zühlsdorf B, Nguyen T-V, Elmegaard B. A comparative assessment of electrification strategies for industrial sites: case of milk powder production. Appl Energy 2019;250:1383–401. https://doi.org/10.1016/j.apenergy.2019.05.071.

[54] Wang SK, Liu C, Zhang SJ, Li QB, Huo ER. Multi-objective optimization and fluid selection of organic Rankine cycle (ORC) system based on economic-environmental-sustainable analysis. Energy Convers Manag 2022;254:17. https://doi.org/10.1016/j.enconman.2022.115238.

[55] Loni R, Najafi G, Bellos E, Rajaee F, Said Z, Mazlan M. A review of industrial waste heat recovery system for power generation with organic Rankine cycle: recent challenges and future outlook. J Clean Prod 2021;287:125070. https://doi.org/10.1016/j.jclepro.2020.125070.

[56] Zühlsdorf B, Jensen JK, Cignitti S, Madsen C, Elmegaard B. Analysis of temperature glide matching of heat pumps with zeotropic working fluid mixtures for different temperature glides. Energy 2018;153:650–60. https://doi.org/10.1016/j.energy.2018.04.048.